

Assessments of structural, hepatotoxicity, cardiotoxicity and genotoxicity of novel synthesized complexes of Sr(II), Ba(II), and Fe(III) with 2,6-dichloroindophenol in male rats

Refat Moamen S.^{1*}, Hamza Reham Z.^{2*}, Adam A.M.A.¹, Saad H.A.¹, Gobouri Adil A.¹, Al-Salmi F.A.², Altalhi T.¹ and El-Megharbel Samy M.¹

1. Department of Chemistry, College of Science, Taif University, P.O. Box 11099, Taif 21944, SAUDI ARABIA

2. Department of Biology, College of Science, Taif University, P.O. Box 11099, Taif 21944, SAUDI ARABIA

*msrefat@yahoo.com

Abstract

Induction of severe hepatic and cardiac damages with saving animal life is a real challenge for the experimental animals. The chlorobenzenes are a small class of cyclic aromatic hydrocarbons. 2,6-Dichloroindophenol is a dye that has been used as a pH and redox indicator for various applications. Previous studies indicate that dichlorobenzene induced relative hepatotoxicity by some degree that did not reach to severe or carcinogenic degree. But in the experimental field, it is a need to induce a severe target toxicity in some experimental animals. In this work we present the synthesis, structural and spectroscopic characterization of strontium(II), barium(II) and iron(III) coordination complexes with 2,6-dichloroindophenol sodium salt hydrate (Dich). The coordination compounds $[Sr(Dich)_2(H_2O)_4]$, $[Ba(Dich)_2(H_2O)_4]$, and $[Fe(Dich)_3(H_2O)_3].4H_2O$ were evaluated on the basis of elemental analyses, molar conductance, infrared and electronic spectra, magnetic measurement, thermal analysis, SEM, and TEM morphological scanning.

All the complexes exhibit an octahedral geometry where the -OH phenolic group coordinates through oxygen and are thermal stable. This study investigated the probable hepatotoxicity and cardiotoxicity of 3 novel complexes groups (Dich/Sr, Dich/Ba and Dich/Fe) (3.6 mmol/Kg) in male rats in addition to control group that was given saline solution as a vehicle. The treatment was (I.P) for successive 30 days. The results indicated sever hepatotoxicity and cardiotoxicity in treated groups with the novel complexes compared to the control group. This was confirmed by low mortality rate in animal groups with elevating Troponin, CPK, ALT, AST, LDH, TNF- α , A-FP, MPO, XO, CRP, SDH, MMP, MDA and lowering antioxidant enzymes (SOD, CAT, GRx and GST) and ATP content in the tissues with incidence of sever hepatic toxicity and structural alteration in liver and heart of treated animals that lead to severe apoptosis of the targeted tissues.

Keywords: Dichloroindophenol, structural, hepatotoxicity, cardiotoxicity, oxidative, antioxidant, histopathology.

Introduction

The benzene chloride compounds are a small type of cyclic hydrocarbon aromatics produced by the substitution of chlorine with a single phenyl ring. The sum of twelve different chlorobenzene isomers have a large scale of physical, chemical and commercial properties¹. 2,6-Dichloroindophenol is a dye which performs as a pH and reduction - oxidation indicator for various applications. DCIP is blue at pH > 7 and pink at pH < 7 and changed to a colorless form². Dichlorobenzene is used for synthesis of organics, manufacturing of dye used as solvent and in chemical industry³. Seventeen countries limit occupational exposure to dichlorobenzene by regulation or recommended guidelines.

Findings from earlier studies indicate that the mechanism which enables certain rat strains to overcome more severe liver injury, is via a biological endogenous compensatory response of the liver resulting in augmented hepatocellular regeneration and tissue repair. A much higher rate of compensatory tissue repair noted in F344 rats compared to S-D rats is suggested to be the mechanism for equalized lethality in the two strains⁴.

This indicates the higher efficiency of the novel complexes (Dich/Ba, Dich/Sr and Dich/Fe) to induce hepatic toxicity with severe degree and save the animal life from lethality and this will be a new point in the incidence of experimental hepatotoxicity and cardiac toxicity. However, the molecular mechanism underlying the increased competency of rats to overcome higher liver injury is not known. What is known is that following liver injury, various molecular events occur which govern the rate and extent of liver regeneration⁵. The relative hepatotoxicity of the dichlorobenzene following (ip) injection has been established⁶. Although the exact mechanism of Dichlorobenzene toxicity is not known, it is said to involve biotransformation resulting in formation of a reactive intermediate⁷. But in the experimental field it did not induce the targeted toxicity for experimental animals as it is not generated before. Choosing of three metal ions (Sr²⁺, Ba²⁺ and Fe³⁺) to be chelated with dichlorobenzene to higher hepatotoxicity was based on some characteristics of these

metals. In the presence of oxygen, cellular Fe enhances reactions that give oxygen reactive species (ORS) in the cytosol and organelles. Low levels of ROS play a role in pathways such as signal transduction, cell proliferation and apoptosis⁸.

The toxicity of barium salts is a function of their aqueous solubility⁹. Barium water-soluble salts such as chloride which are used in the current study produce a variety of acute toxic effects in humans and experimental animals involving the cardiovascular, gastrointestinal and hematopoietic systems¹⁰. The most characteristic toxic signs resulting from barium ingestion involve an intense stimulation of smooth, striated, and cardiac muscle¹¹. Prolonged exposures to barium are reported to produce muscle weakness¹². Sr element has low toxicity effect. The Sr ion is present in tissue of animal in 0.01-1 ppm. The accumulation of Sr is related to the amount of Ca which is a vital element in relation to heart mechanism of action. The absorption of strontium in the gastrointestinal tract is normally poor¹³.

Induction of severe hepatic and cardiac damages with keeping animal life is a real challenge for the experimental animals. Despite higher incidence of liver injury of dichlorobenzene novel complexes, it is a must to reduce the rats' lethality to guarantee the success of the experiments. Thus, this study aimed to assess the hepatic and cardiac toxicity induced by the novel synthesized complexes and evaluate their severe toxicity on different physiological and structural alterations in liver and heart.

Material and Methods

Chemical and Analyses: All reagent grade chemicals and solvents, 2,6-dichloroindophenol sodium salt hydrate (Dich), SrCl₂.6H₂O, BaCl₂.2H₂O, and FeCl₃.6H₂O were purchased from Sigma-Aldrich with high degree of purity.

Synthesis of (DICH) coordination compounds: [Sr(Dich)₂(H₂O)₄], [Ba(Dich)₂(H₂O)₄] and [Fe(Dich)₃(H₂O)₃].4H₂O, were prepared by mixing appropriate salts (SrCl₂.6H₂O, BaCl₂.2H₂O, or FeCl₃.6H₂O) (1 mmol) dissolved in 20 ml of distilled water to Dich (2 mmol or 3 mmol), (1:2 or 1:3 molar ratio) dissolved in 20 ml of methanol, and refluxed for three hours. The product was allowed to stand for two days at room temperature. The product coordinated complexity was characterized and explained by lot of spectral and chemical instruments (FTIR, UV, C,H,N analysis, TG and magnetic susceptibility measurements).

[Sr(Dich)₂(H₂O)₄] complex (Dich/Sr): A Dich solution (0.581 g, 2 mmol) in CH₃OH (20 ml) was added to an aqueous solution of SrCl₂.6H₂O (0.267 g, 1 mmol) (20 ml). The mixture was heated under reflux for 3 hours. A microcrystalline color with bluish black was formed by slow evaporation of solvent and it was filtered and dried under vacuum over anhydrous CaCl₂. Anal. Calc. for C₂₄H₂₀Cl₄N₂O₈Sr: C, 41.54%; H, 2.91%; N, 4.04%. Found:

C, 41.23%; H, 2.85%; N, 3.97%. Melting point > 250 °C and the yield is 74%.

[Ba(Dich)₂(H₂O)₄] complex (Dich/Ba): A Dich solution (0.581 g, 2 mmol) in CH₃OH (20 ml) was added to an aqueous solution of BaCl₂.2H₂O (0.245 g, 1 mmol) (20 ml). The mixture was heated under reflux for 3 hours. A microcrystalline precipitate with bluish black color was formed by slow evaporation of the solvent and it was filtered and dried under vacuum over anhydrous CaCl₂. Anal. Calc. for C₂₄H₂₀BaCl₄N₂O₈: C, 38.77%; H, 2.71%; N, 3.77%. Found: C, 38.64%; H, 2.55%; N, 3.45%. Melting point > 250 °C and the yield is 77%.

[Fe(Dich)₃(H₂O)₃].4H₂O complex (Dich/Fe): A Dich solution (0.871 g, 3 mmol) in CH₃OH (20 ml) was added to an aqueous solution of FeCl₃.6H₂O (0.271 g, 1 mmol) (20 ml). The mixture was heated under reflux for 3 hours. A microcrystalline precipitate with brownish black color was formed by slow evaporation of the solvent and it was filtered and dried under vacuum over anhydrous CaCl₂. Anal. Calc. for C₃₆H₃₂Cl₆FeN₃O₁₃: C, 43.98%; H, 3.28%; N, 4.27%. Found: C, 43.77%; H, 3.19%; N, 4.22%. Melting point > 250 °C and the yield is 69%.

Type of analysis	Models
Elemental analyses	Perkin Elmer CHN 2400
Conductance	Jenway 4010 conductivity meter
FTIR spectra	Bruker FTIR Spectrophotometer
Electronic spectra	UV2 Unicam UV/Vis Spectrophotometer
Magnetic moment	Magnetic Susceptibility Balance
Thermo gravimetric	TG/DTG-50H, Shimadzu thermo-gravimetric analyzer
SEM	Quanta FEG 250 equipment
TEM	JEOL 100s microscopy

Animals and experimental protocol: Animal experiments have been set following the approval of Taif University Animal Ethical Committee. The experimental animals were healthy, adult male albino rats weighing 180–200 g. The animals were housed with food and water *ad libitum* under a 12 hrs light/dark cycle to decrease the suffering. Forty male rats were divided into 4 groups (10 in each). The healthy control non-treated group were treated with a saline solution as a vehicle. No intervention was carried out in any of the animals after the injection and during the experimental period. There has also been no use of analgesics or anti-inflammatory drugs. The other three groups (Dich/Sr, Dich/Ba and Dich/Fe) were injected as previously described to the dose of dichlorobenzene (3.6 mmol/Kg)¹⁴. The experiment period was carried for 30 successive days.

Hepatic function activities and biomarkers: Protein levels were evaluated according to Bradford¹⁵ and Kaplan and Szalbo¹⁷. ALT, AST and ALP levels were assessed by using (SENTINEL CH) kits. LDH levels were measured according to King¹⁶.

Determination of the proinflammatory biomarkers:

Blood samples were collected for determination of serum pro-inflammatory biomarkers at the end of the experiment. Serum levels of tumor necrosis factor-alpha (TNF- α) and Alpha Fetoprotein were measured according to No. R6365 and RB1829 respectively (ELISA kit BIOTANG INC, Cat. MA, USA) as recommended by the manufacturer.

Estimation of inflammation biomarkers: C-reactive protein (CRP) was determined by the method of Wener et al¹⁸ using Enzyme-linked Immunosorbent Assay Kit (SEA821).

Determination of enzymatic antioxidant biomarkers:

CAT activity was determined according to Aebi¹⁹. SOD was estimated according to Marklund and Marklund²⁰. MDA levels were estimated according to Ohkawa et al²¹. GST was evaluated according to Couri and Abdel-Rahman²² and GRX was evaluated according to Glodberg and Spooner²³.

Determination of MPO and XO: MPO is present excessively in the neutrophil granulocytes²⁴, MPO kits provide reliable results. XO was assayed according to Litwack et al²⁵.

Preparation of liver tissues homogenate: Small portions of the hepatic tissues (~0.25 g) were used to assess the oxidative stress injury. Hepatic tissues were embedded in ice saline Na₂HPO₄/NaH₂PO₄ buffer with pH 7.4/g tissues by using tissue homogenizer. The resultant supernatant after tissue homogenization was transferred into the Eppendorf tubes and kept at -80 °C.

Mitochondrial potential function

Evaluation of succinate dehydrogenase: Metabolic viability based assays using tetrazolium salts like MTT (3-(4,5-Dimethylthiazol 2-yl)-2,5-diphenyltetrazolium bromide) are used for measuring the mitochondrial metabolic rate and indirectly reflect the viable cell numbers. The mitochondrial SDH activity was evaluated using molecular probe MTT. Mitochondrial suspensions from the knee joints were incubated with MTT probe (0.4% w/v) for 30 min at 30 °C. Then, 100 μ L dimethyl sulfoxide (DMSO) was used to dissolve the formazan crystals. The total amount of formazan produced upon MTT reduction is directly proportional to the number of viable cells. Finally, the absorbance was measured using an ELISA reader at 570 nm (Tecan, Rainbow Thermo, Austria)²⁶.

Mitochondrial ROS assay: The mitochondrial ROS generation was evaluated using the dichlorodihydro fluorescein diacetate (DCFH-DA) probe. Mitochondrial suspensions from the knee joints were incubated with DCFH-DA probe at a final concentration of 10 μ M for 30 min at 30 °C. Finally, the fluorescence intensity of dichlorofluorescein (DCF) was measured using the Shimadzu RF-5000 U. fluorescence spectrophotometer (λ Ex = 488 nm, and λ Em = 527 nm). An increase in

fluorescence intensity indicates an increase in the generation of ROS due to exposure to inflammation of hepatotoxicity and cardiotoxicity²⁷.

Mitochondria membrane potential (MMP, $\Delta\Psi$ M) Assay:

The mitochondria of hepatic and cardiac tissues were isolated from all groups. Briefly, the mitochondrial ROS generation was evaluated using rhodamine 123 (Rh123) probe at a final concentration of 10 μ M for 30 min at 30 °C. Finally, the collapse of MMP was evaluated using Shimadzu RF-5000 U fluorescence spectrophotometer (λ Ex = 490 nm and λ Em = 535 nm). An increase in fluorescence intensity indicates an increase in the collapse of MMP²⁸.

Evaluation of swelling on mitochondria: Briefly, swelling on mitochondria in sizes of 10 and 100 nm (pure and impure) was measured using an ELISA reader (Tecan, Rainbow Thermo) at 540 nm. A decrease in absorbance indicates an increase in mitochondria swelling²⁸.

Cytochrome-C oxidase release assay: Evaluation of cytochrome c release (complex IV) that referred to mitochondrial volume was measured (Quantikine Rat/Mouse cytochrome c Immunoassay kit, R and D Systems, Inc., Minneapolis, MN, USA).

ATP content assay: The ATP content was detected using the luciferase enzyme. The intensity was evaluated using Sirius tube luminometer (Berthold Detection System, Germany). ATP content was expressed as nmol/mg protein²⁹.

GSH content assay: GSH content was determined for isolated mitochondria using DTNB as the indicator and spectrophotometer (UV-1601 PC, Shimadzu, Japan). The mitochondrial was added into 0.1 mol/L of phosphate buffers and 0.04% DTNB in a total volume of 3.0 mL (pH 7.4). The developed yellow color was read at 412 nm. GSH content was expressed as μ g/mg protein³⁰.

Lipid peroxidation (LPO) assay: The malondialdehyde (MDA) content was evaluated to measure LPO. The level of MDA was measured in the supernatant at 532 nm using an ELISA reader (Tecan, Rainbow Thermo, Austria). Furthermore, MDA content was expressed as μ g/mg protein. An increase in MDA content indicates an increase in LPO level³¹.

Myeloperoxidase and xanthine oxidase activities: MPO and XO were detected spectrophotometrically according to Suzuki et al²⁴ and Litwack et al²⁵ respectively.

Estimation of Troponin, CK-MP and CK: It was determined in the serum by using BQ-Kits according to the manual of procedure.

Histological and TEM microscopic examination: A liver portion was kept in 10% neutral buffered formalin and then completed other processing according to Gabe³².

Transmission electron microscope (TEM) study: Liver and heart specimens were dissected and TEM sections were obtained after fixation in 2.5 % glutaraldehyde and other procession to form resin capsule³³. Tissue blocks were cut serially into ultrathin (0.07 mm) sections which were stained with uranyl acetate at 4°C for 2 h and lead citrate at 4°C for 20 min. Sections were subsequently observed under transmission electron microscopy (JEOL JSM-5600LV-Japan, magnification, ×12,000) Faculty of Agriculture, Mansoura University in Mansoura city, Egypt.

RNA isolation and RT-PCR analysis: Total RNA was isolated from the hepatic cells by using Trizol reagent (Invitrogen). RNA was preserved at -80 °C. RNA (1 µg) was used for reverse transcription reaction using reverse transcriptase, reverse primer, deoxyribonucleotide triphosphate and 1U RNase inhibitor. The reaction was incubated at 42°C for 1 h. The PCR reactions were carried out in a total volume of 20 µl containing *Taq* DNA polymerases, 0 dNTP, reaction buffer and forward and reverse primers as follows:

	Forward	Reverse
COX-2	5'-CCC-AGAGCT-TTT-CAA-CC-3'	5'-ATT-TGG-CAC-ATT-TCT-TCC-CC-3'
iNOS	5'-CCC-TTC-CGA-AGT-TTC-TGG-CAG-CAG-C-3'	5'-GGC-TGTCAG-AGC-CTC-GTG-GCT-TTG-G-3'
TNF-α	5'-AGC-ACA-GAA-AGC-ATGATC-CG-3'	5'-GTT-TGC-TAC-GAC-GTG-GGC-TA-3'
IL-6	5'-CGA-TGA-TGC-ACT-TGC-AGA-AA-3'	5'-TGG-AAA-TTG-GGG-TAGGAA-GG-3'
IL-1β	5'-TGC-AGA-GTT-CCC-CAA-CTG-GTA-CAT-C-3'	5'-GTG-CTG-CCT-AAT-GTC-CCC-TTG-AAT-C-3'
β-Actin	5'-TCATGA-AGT-GTG-ACG-TTG-ACA-TCC-GT-3'	5'-CCT-AGA-AGC-ATTTGC-GGT-GCA-CGA-TG-3'

After the initial denaturation at 95 °C, the amplification by 35 cycles of 93 °C for 40 seconds (denaturing), 50-52 °C for 40 sec (annealing), 73 °C for 40 sec (extension) occurred. The PCR products were analyzed by 1.5% agarose gel electrophoresis. The mRNA expression level was quantitated by (Bio-Rad) Quantity One software.

Illustrative 3D parametric ECG: Male rats of treated groups with these novel complexes Dich/Sr, Dich/Ba and Dich/Fe were anaesthetized during the experimental period by thiobarbital and then using the electric poles and injection of saline solution in the Jugular vein during estimation of heart beats and then using (Lab chart) software and then recording the illustrative data.

Comet assay: Pieces of the heart of control and treated groups were placed into a small Petri dish with a cold solution (Ca²⁺, Mg²⁺ free HBSS, 10% DMSO and 20 mM EDTA). The comet assay was performed as described by Endoh et al³⁴.

Statistical analysis: For statistical calculations, the SPSS 22.0 software program was used. Data were presented as mean ± standard error. Differences between groups were assessed through a one-way Analysis of Variance followed by post hoc Duncan test ($P < 0.05$).

Results

Structure interpretations of Sr^{II}, Ba^{II} and Fe^{III} Dich complexes

Conductance measurements: The purity of the synthesized Dich complexes was checked by elemental analysis, FTIR and SEM. Physical and microanalytical characteristics of these metal complexes are given above. The strontium(II), barium(II) and iron(III) Dich complexity are dissolved in dimethyl formamide, and dimethyl sulfoxide and are insoluble in methanol, ethanol, acetone, CHCl₃ and water.

The elemental analysis data of the complexes is consistent with the calculated results from the empirical formula of each compound (S1). The observed molar conductances of the complexes in DMSO for 10⁻³ M solutions at room temperature are consistent with the non-electrolytic nature (9-14 ohm⁻¹.cm².mol⁻¹) of the complexes³⁵.

Infrared spectroscopy: The main characteristic infrared spectral bands (cm⁻¹) are in S1. To study the mode of coordination of Dich ligand to the metals in the complexes, the infrared spectrum of ligand (Fig. 1a) was compared with the spectra of the complexes (Fig. 1b). IR spectra of the 2,6-dichloroindophenol sodium salt hydrate (Dich) has the most characteristic bands appearing at 3376 and 3144 cm⁻¹ ν(O-H) hydrated water molecules, 2954, 2762 and 2735 cm⁻¹ ν(C-H) two aromatic rings (2,6-dichloro-4-imino-cyclohexa-2,5-dienone and phenolic), 1631 cm⁻¹ ν(C=O) of 2,6-dichloro-4-imino-cyclohexa-2,5-dienone ring, 1589 cm⁻¹ ν(C=N), 2,6-dichloro-4-imino-cyclohexa-2,5-dienone ring, 1564-1428 cm⁻¹ ν(C=C) aromatic, ν_{as}(C-N-C), ν_s(C-N-C) of the functional group at 1311 and 1174 cm⁻¹ respectively, 1256 cm⁻¹ ν(C-O), and 867-614 cm⁻¹ ν(C-Cl) halo organic compound.

Sr(II), Ba(II) and Fe(III) complexes give a broad band at 3487-3197 cm⁻¹ and a new band at 790-761 cm⁻¹. These bands may be attributed to the vibrations of coordinated water molecules. The band at 1631 cm⁻¹ due to the presence of the carbonyl group of the 2,6-dichloro-4-imino-cyclohexa-2,5-dienone ring is shifted to higher frequencies (1717-1700 cm⁻¹) after complexation indicating that the Dich ligand is not coordinated to metal ions (Sr²⁺, Ba²⁺, and Fe³⁺) by the carbonyl oxygen atom but only by the phenolic oxygen³⁶⁻³⁸ referring to bonding of the unsaturated oxygen of the phenolic group with metal ion³⁶ and chelation occurs by the electrons donation from oxygen to the empty *d*-orbitals of the metal atom. The phenolic C-O stretching vibrations that appeared at 1256 cm⁻¹ in the Dich chelat³⁸ are shifted towards lower frequencies by ~ 20 cm⁻¹ in the complexes (S1).

This decrease in wave number refers to involving of oxygen in the C–O–M bond. In the low frequency region, the band of medium intensity observed for the complexity at 550–501 cm^{-1} characterized to $\nu(\text{M–O})$ ³⁸. Other differences in the spectra of the divalent Sr, Ba and trivalent Fe complexity include a shift in a peak from 1564–1428 cm^{-1} to 1565–1400 cm^{-1} assigned to C=N and C=C ring stretching³⁹; shifting of peak wavenumbers may be due to functional neighboring groups or its conjugation as well as changes in density of electron. If atoms neighboring give density of electron to the functional group, a higher absorbance shifts in peak will occur, while lower absorbance shifts in peak will occur when decreasing density electron⁴⁰.

All the infrared spectra of Dich ligand and its metal complexity imply that the Dich acts as monodentate and coordinated to M^{+n} through O of phenolic OH ring moiety (Fig. 1 a, b).

Electronic and magnetic measurements: The diffuse reflectance spectrum of iron(III) complex $[\text{Fe}(\text{Dich})_3(\text{H}_2\text{O})_3] \cdot 4\text{H}_2\text{O}$ has been taken in solid state. The electronic spectrum of the complex exhibit three electronic absorption bands at 519, 435, and, 392 nm which may be due to electronic transitions ${}^6\text{A}_{1g} \rightarrow {}^4\text{T}_{1g}$, ${}^6\text{A}_{1g} \rightarrow {}^4\text{T}_{2g}$, ${}^6\text{A}_{1g} \rightarrow {}^4\text{A}_{1g}$, ${}^4\text{E}_g$, respectively⁴¹ and suggests octahedral geometry. The magnetic moment of the iron(III) complexity is 5.42 B.M. that is in a good agreement with six-coordinated iron(III) complexes and consistent with the presence of five-unpaired electrons⁴².

The Dich is black blue in color, and this color has a maximum wavelength at λ_{max} 629 nm. This band clearly existed in the three complexes which shifted to higher wavelength at about ~ 643 nm under complexation (Fig. 1 C). The magnetic susceptibilities data of divalent Sr and Ba complexity have a diamagnetic nature as expected for a d^{10} system i.e. paired electron in valence shell orbital or invisibility of unpaired electron.

Thermal analysis: Sr(II), Ba(II) and Fe(III) complexes give a mass loss in within region 80–200 °C corresponding to uncoordinated and coordinated H_2O molecules present in the synthesized complexes (e-component). The complexity not gave loss in mass up to 600 °C, this reveals that thermal stability. The TG curves in the 200–600 °C range with DTG_{max} at 368, 433 and 565 °C, 325 and 534 °C and 310, 458 and 594 °C in case of Sr(II), Ba(II), and Fe(III) respectively and suggested that the mass loss for all three complexes was due to loss of Dich ligand. The remaining of ignition are metal oxides (SrO, BaO, and FeO).

These results confirm the loss of the complexity, mass loss (Calc. Found for $[\text{Sr}(\text{Dich})_2(\text{H}_2\text{O})_4]$, $[\text{Ba}(\text{Dich})_2(\text{H}_2\text{O})_4]$, and $[\text{Fe}(\text{Dich})_3(\text{H}_2\text{O})_3] \cdot 4\text{H}_2\text{O}$ as (85.07) 84.50%, (79.38) 79.00% and (92.69) 91.50% respectively.

SEM and TEM morphological investigations: The particle size and morphology of the Sr(II), Ba(II) and Fe(III) Dich complexes have been under investigation by SEM and TEM. Fig. 3a–c and fig. 3d–f depict the SEM and TEM photographs of the synthesized Sr(II), Ba(II), and Fe(III) complexes. There is a uniform matrix of the synthesized novel complexes in the images. This can be deduced that the synthesized complexes material have a homogeneous phase. A slices like shape is observed in the Sr(II) complexity (Fig. 2a) with size particle of 5 μm .

The single phase formation of Ba(II) complexity having rectangular pieces morphologies with particle size 5 μm is shown in fig. 2b. The image of iron(III) complexity (Fig. 2c) gives sheets like shape with particle size 5 μm . Figures 5d–f show the TEM images of the prepared Dich nanoparticles complexes, these indicate that Sr(II), Ba(II) and Fe(III) nanoparticle complexes are approximately spherical or of semispherical shape with the diameter within 10–22 nm, 15–30 nm, and 36–46 nm respectively.

Biological results

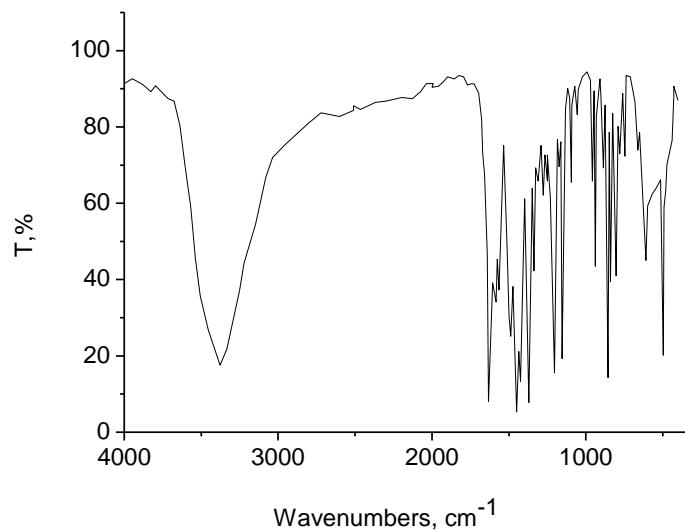
Mortality rate: Dich/Sr, Dich/Ba and Dich/Fe administration in male rats for successive 30 days resulted in low mortality rate (S1) represented by 1.02, 0.8 and 0.7% which is considered low rate compared to the size of sever toxicity induced by the used novel complexes. The high rate between treated groups was Dich/Sr group.

Liver functions: Dich/Sr, Dich/Ba and Dich/Fe administration in male rats for successive 30 days resulted in significant increment in serum AST and ALT levels as compared with control group. The high significant increase in hepatic enzyme markers was recorded in Dich/Fe treated group. Dich/Sr, Dich/Ba and Dich/Fe administration afforded a marked elevation in LDH levels as compared with the control group (e-component).

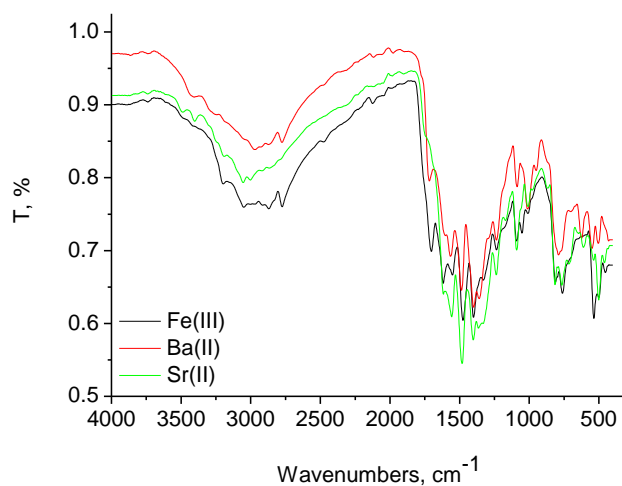
Serum TNF- α activity: Administration of Dich/Sr, Dich/Ba and Dich/Fe elicited a significant increment in serum TNF- α and AFP levels whereas the higher record was in rat group treated with Dich/Fe (e-component).

Oxidative stress biomarkers: Dich/Sr, Dich/Ba and Dich/Fe administration caused a marked decrement in CAT, SOD, GRx and GST levels as compared with the control group (Table 1) and the highest decrement was recorded in Dich/Fe treated group while induced significant increment in MPO and XO levels was shown in e-component.

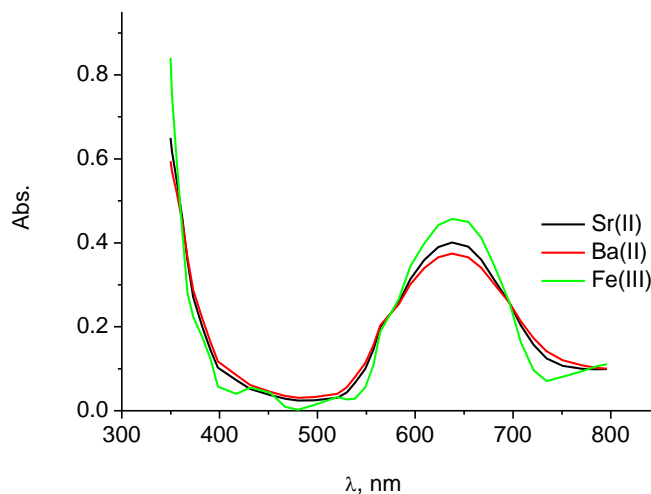
MDA levels were increased significantly after administration of Dich/Sr, Dich/Ba and Dich/Fe treatment as compared with those in the control group and its level was significantly increased in Dich/Fe treated group. Meanwhile, Dich/Sr, Dich/Ba and Dich/Fe treated groups induced remarkable decrement in liver GRx levels as compared with the control group.



(a) Infrared spectrum



(b) Infrared spectrum



(c) UV-Vis spectrum

Fig. 1 (a, b, c): (a) Infrared spectrum of Dich free ligand, (b) Infrared spectrum of Sr^{II}, Ba^{II}, and Fe^{III} Dich complexes and (c) UV-Vis spectrum of Sr^{II}, Ba^{II} and Fe^{III} Dich complexes

GST activity was significantly decreased in Dich/Sr, Dich/Ba and Dich/Fe treated groups as compared with the control group. MPO and XO rose to 41.73, 46.87 and 51.42 fold in Dich/Sr, Dich/Ba and Dich/Fe treated rats as compared to control healthy animals respectively (e-component). The highest increment was recorded in Dich/Fe treated group which appeared to decline significantly in control group (Table 4). Treatment the rats with Dich/Sr, Dich/Ba and Dich/Fe significantly decreased the activities of XO by 50.25 %, 54.58 and 58.22 % respectively. However,

the significant increase was recorded in the Dich/Fe treated group.

Cardiac Bio-Markers (Troponin, CK-MP and CPK) levels: Dich/Sr, Dich/Ba and Dich/Fe administration induced a significant increment in Troponin, CK-MP and CPK levels as compared with the control group (e-component) and the highest increment of previous markers indicate abnormal heart functions and incidence of tachycardia case.

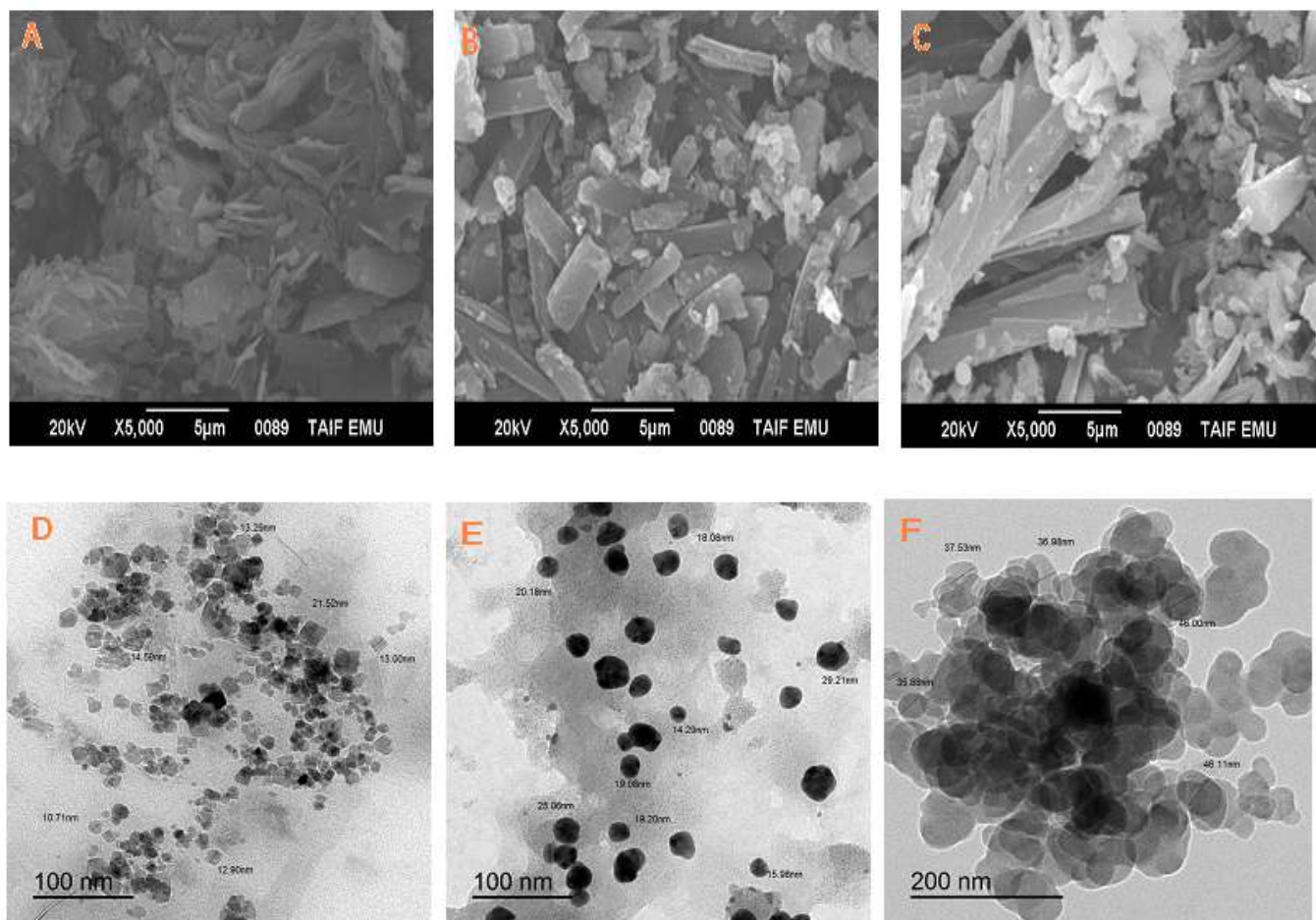


Fig. 2: SEM and TEM images of A and D: Sr^{II}, B&E: Ba^{II}, and C and F: Fe^{III} Dich complexes

Table 1
Changes in oxidative/antioxidant parameters of antioxidant enzymes of control and treated rats with Dich/Sr, Dich/Ba and Dich/Fe.

Groups	Parameters				
	CAT (U/g)	SOD (U/g)	MDA (U/g)	GRx (U/g)	GST (U/g)
Control	3.9 ± 0.5 ^a	21.4 ± 2.2 ^a	2.21 ± 0.4 ^d	26.3 ± 3.2 ^a	20.7 ± 1.5 ^a
Dich/Sr	0.9 ± 0.1 ^{bc}	8.9 ± 1.6 ^b	57.3 ± 3.2 ^c	9.2 ± 1.2 ^b	5.7 ± 0.8 ^b
Dich/Ba	0.8 ± 0.5 ^c	8.9 ± 2.7 ^b	119.3 ± 3.5 ^b	8.3 ± 1.3 ^c	4.9 ± 0.9 ^{cd}
Dich/Fe	0.72 ± 0.2 ^d	7.6 ± 3.5 ^c	135.4 ± 4.4 ^a	7.9 ± 1.7 ^d	4.2 ± 0.7 ^d

Means within the same column in each category (mean ± SE and n = 10) carrying different letters are significant at P ≤ 0.05 using Duncan's multiple range test, where the highest mean value has symbol (a) and decreasing in value were assigned alphabetically. SOD:Superoxide dismutase; MDA:Malondialdehyde; CAT:Catalase; GRx:Glutathione reductase; GST: Glutathione-S-transferase.

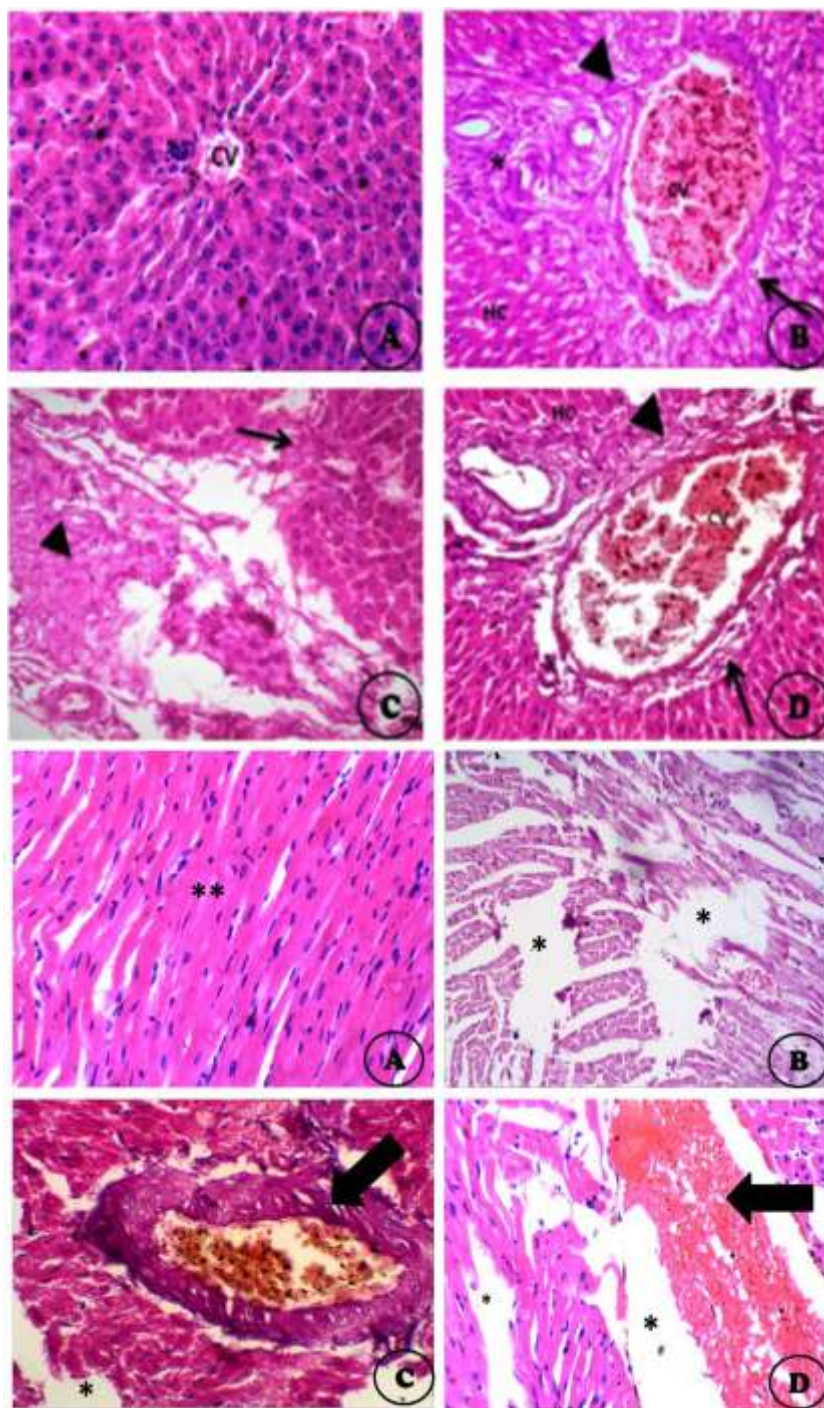


Fig. 3: (a) Histological sections of liver tissues. Fig (A) Photomicrograph of sections of liver showed normal hepatic tissues with normal nucleus (H and Ex200).Fig (B) Photomicrograph of sections of liver of (Dich/Sr) treated group showed markedly dilated central vein (CV) lies at the center of the lobule surrounded by the hepatocytes (HC) pericentral zone shows necrotic hepatocytes (arrows) with portocentral fibrosis (arrow head) with infiltration with lymphocytes (*) (H and Ex200). Fig (c) Photomicrograph of sections of liver of (Dich/Ba) treated group showed markedly distortion of lobular architecture, wide areas of fibrosis (arrow head), hepatocytes showed degeneration and apoptotic bodies (arrow) (H and E x200).Fig (D) Photomicrograph of sections of liver of (Dich/Fe) treated group showed markedly dilated central vein (CV) lies at the center of the lobule surrounded by the hepatocytes (HC). Pericentral zone shows necrotic hepatocytes (arrows) with bands of fibrous tissue (arrow head) (H and E x200). (b) Histological sections of cardiac tissues (Left ventricle). Fig. (A) Control group showing normal cardiac myocytes ()(H and E X 400). (B) Dich/Sr treated group showing severe myocyte necrosis with ruptured muscle bundles(*) (H and E X 400). (C) Dich/Ba treated group showing highly severe cardiac infarction with appeared fibrotic lesion with appeared congestion (Black arrow) (H and E X 400). (D) Dich/Fe treated group showing severe rupture of cardiac bundles (*) with severe congestion (Black arrow) (H and E X 400).**

TNF- α , AFP and CRP levels in the serum: The levels of cytokine TNF- α and AFP in the serum were detected on day 30 after induction of toxicity by Dich/Sr, Dich/Ba and Dich/Fe treatment (e-component). They significantly increased in the mentioned treated groups compared with the healthy control animals. Serum CRP level in control rats at baseline was 3.05 ± 0.7 mg/L with a significant difference by 47.0, 68.0 and 82-fold and Dich/Sr, Dich/Ba and Dich/Fe treated rats (S1). Importantly, there was a more significant increment in CRP level in rats treated with Dich/Fe with 92.36 % as compared to the control group.

SDH, ROS, and MMP: The cell viable number detected by SDH% is presented in fig. 4. The SDH was 94.4% in normal control animals and decreased significantly to 52.36%, 45.25% and 38.59 % in Dich/Sr, Dich/Ba and Dich/Fe treated groups. The values of ROS were 90.36%, 95.69%, and 99.36% in animals treated with Dich/Sr, Dich/Ba and Dich/Fe respectively in fig. 4. The baseline value of MMP ($\Delta\psi_m$) for normal healthy rats was 0.4 ± 0.01 as shown in S1. The Dich/Sr, Dich/Ba and Dich/Fe treated rats presented higher ROS content than controls for mitochondria. Dich/Sr, Dich/Ba and Dich/Fe administration accelerated mitochondrial swelling and Cytochrom-C as illustrated in fig. 5 where it was elevated significantly as compared to control healthy rats. Dich/Sr, Dich/Ba and Dich/Fe treated rats release less ATP content (45.8%, 42.25% and 35.58%) as compared to control rats (S1).

Gross section of hepatic tissues: S1 clarified some gross live section of severe damages and toxicity induced by the novel complexes Dich/Sr, Dich/Ba and Dich/Fe which were represented by hepatic nodules and appearance of dark black spots changing in hepatic eco-structures with severe oxidative stress in hepatic and cardiac tissues.

Histological evaluation: Histological sections of liver tissues are given in fig. 3a. (A) Control group is showing normal hepatic tissues with normal nucleus (H and Ex200). (B) Dich/Sr treated group showed markedly dilated central vein lying at the center of the lobule surrounded by the hepatocytes pericentral zone shows necrotic hepatocytes with portocentral fibrosis with infiltration with lymphocytes (H and Ex200). (C) Dich/Ba treated group showed markedly distortion of lobular architecture, wide areas of fibrosis, hepatocytes showed degeneration and apoptotic bodies (H and E x200). (D) Dich/Fe treated group showed markedly dilated central vein lying at the center of the lobule surrounded by the hepatocytes. Pericentral zone shows necrotic hepatocytes with bands of fibrous tissue (H and E x200).

The histological sections of cardiac tissues (Fig. 3 b) showed (A) control group showing normal cardiac myocytes (B) Dich/Sr treated group showing severe myocyte necrosis with ruptured muscle bundles (C) Dich/Ba treated group showing highly severe cardiac infraction with appeared fibrotic lesion with appeared congestion and (D) Dich/Fe treated group

showing severe rupture of cardiac bundles with severe congestion .

Electron microscope evaluation: Furthermore, the present study was to identify whether Dich/Sr, Dich/Ba and Dich/Fe induced severe damages in both heart and liver and affects on their structures (Fig. 6 a). The healthy (A) control group is showing normal hepatic structure with appearance of large round nucleus with homogenous euchromatin and mitochondria and normal sized endoplasmic reticulum. (B) Dich/Sr group is showing hepatic tissues Laceration with disappearance of most of hepatic structures and functional organelles, Appearance of nucleus in very necrotic form as a crescent is formed with irregularly boundaries. (C) Dich/Ba group is showing degeneration of most hepatic structures with mild necrotic nucleus with irregular boundaries, appearance of degenerated endoplasmic reticulum and degenerated mitochondria and appearance of red blood cells and destingration of most hepatic tissues (**).(D) Dich/Fe group is showing disappearance of the nucleus which revealed the occurrence of apoptosis with large sized red blood cells with degeneration of most hepatic structures with disappearance of mitochondria crista.

Meanwhile, TEM sections of heart tissues (Fig. 6 b) showed (A) control group showing control heart showing cardiomyocytes that have a tightly organized sarcomeric structure containing a peripheral nucleus with regular chromatin; the Z-lines are clearly visible and normal mitochondria are clear within myofiber, and integrity intercalated disc . (B) Dich/Sr group showing the cardiomyocytes has a disorganized sarcomeric structure along with appearance of intercellular spaces. In addition, another interesting observation was the abnormal accumulation of mitochondria within myofibers and destroyed intercalated disc. (C) Dich/Ba group is containing abnormal nucleus with irregular membrane and abnormal chromatin.

Some fibers exhibited a complete lack of organization with Z-lines that appeared to be dissolving or fragmented and myofibrils and appeared lesion in cardiac myofibril separated in fascicles by the sarcomeres. (D) Dich/Fe treated group showing Z-lines exhibited various types of morphologies. Some Z-lines were extremely thick, round, and highly electron dense whereas others were punctate and appeared fragmented.

3D ECG Lab chart of groups treated with (Dich/Sr, Dich/Ba and Dich/Fe): Illustrative 3D parametric ECG displays of radial velocity with the Lab chart software (Fig. 7a). (A) Control group showing normal heart beats with the characteristic points (P, Q, R, S, T) is showing normal signal as (P) represents contraction of the heart and movement of blood from up down the heart, (QRS) represents the ventricle contraction and appears upper than other signals. (T) represents the relaxation of the heart and pulse end with normal waves and appearance of rich oxygenated red colour

without waves with regular waves. (B) Dich/Sr group is showing blue colour which indicates incidence of oxidative stress and wavy in (P and T) waves with appearance of faint blue colour which indicates cardiac cells necrosis and area of non-clearance flow.

(C) Dich/Ba is showing more wavy appearance of signals of heart with irregular waves in (P and T waves) (Green and Black arrows) that indicates up normal blood flow with faint colour in T wave which indicates necrotic cardiac tissues(*). (D) Dich/Fe is showing irregular heartbeats waves (wavy chart) with high faint blue color of T wave which indicates more cardiac damages.

Electrocardiograms (ECG) (Fig. 7b) changes in rats in different treated groups are shown: (A) control group is showing normal P waves with normal interval of 0.14 sec. (B) Dich/Sr treated group is showing case of ventricular tachycardia as this chart is distinguished in diagnostic of

ventricular tachycardia showing ventricular aberration which occurs in short repeated bursts separated by appeared two sinus (intervals black arrow) with appearance atrial flutter (F) which is recognized by the presence of "saw tooth" with average intervals of 0.10 sec. (C) Dich/Ba treated group showing treated group is showing also a case of ventricular tachycardia with appearance ventricular aberration which occurs in this group by very short repeated bursts (very narrow peak), separated by appeared narrow two sinus (intervals black arrow) with appearance atrial flutter (F) which is recognized by the presence of "saw tooth" with average intervals of 0.8 sec.

(D) Dich/Fe treated group is showing high case of ventricular tachycardia which is known as repetitive tachycardia (Red circle) with short beat intervals (intervals black arrow) and appearing as ventricular fusion beats (Black circle) with the fusion of beats with average intervals of 0.9 sec.

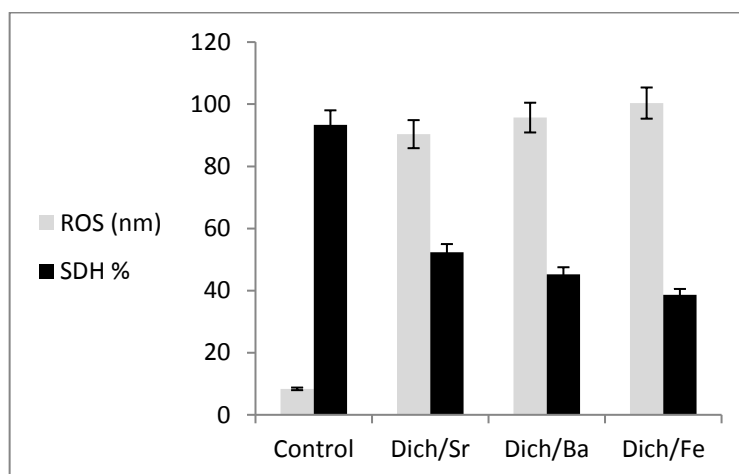


Fig. 4: The elevation of succinate dehydrogenase (SDH) and reactive oxygen species (ROS) in the liver homogenates of rat model treated with control and treated rats with Dich/Sr, Dich/Ba and Dich/Fe. The data presented as mean \pm S.E.

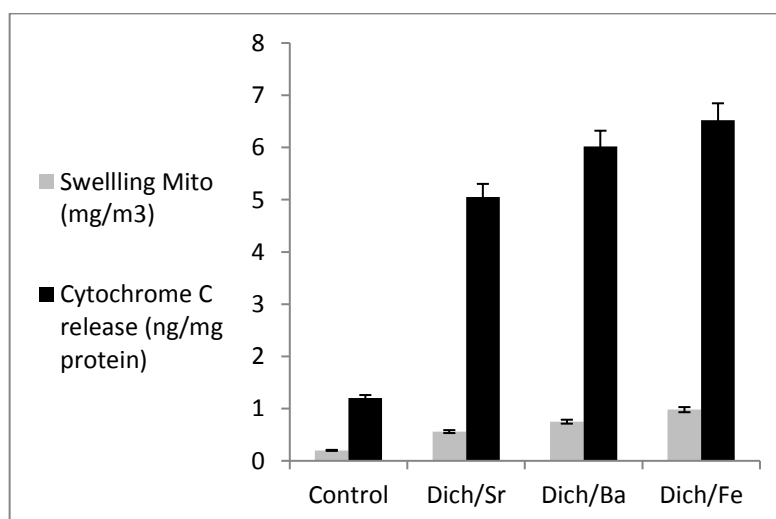


Fig. 5: The elevation of swelling mitochondria and cytochrome C release in the liver homogenates of rat model treated with control and treated rats with Dich/Sr, Dich/Ba and Dich/Fe. The data presented as mean \pm S.E.

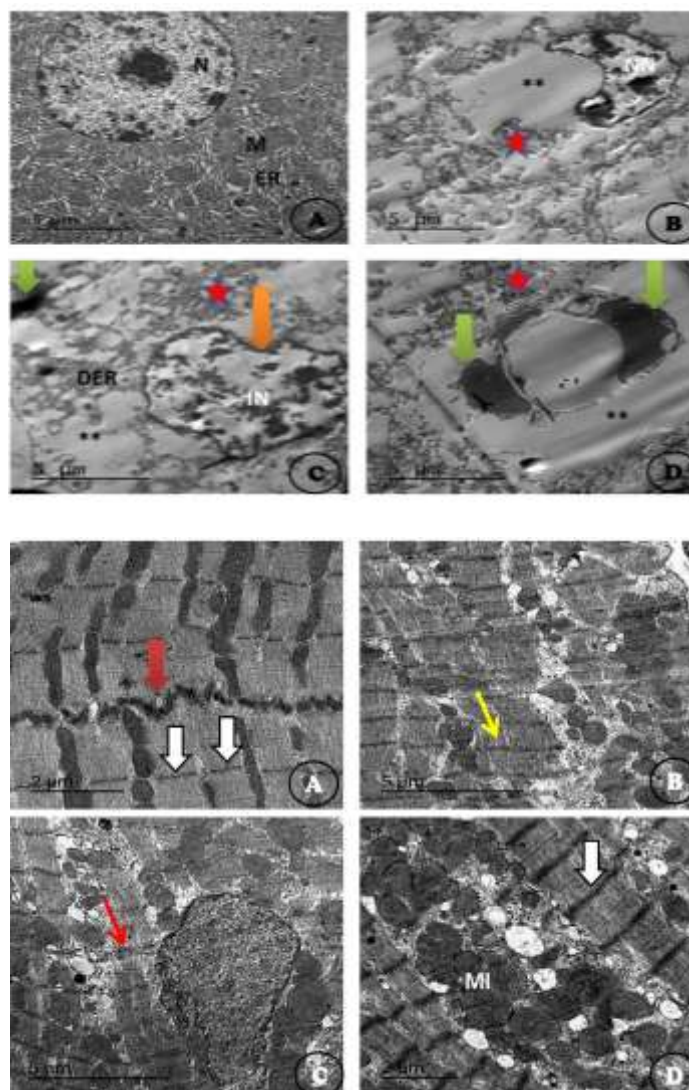


Fig. 6: (a) Transmission Electron microscopy of sections of (A) control group showing normal hepatic structure with appearance of large round nucleus (N) with homogenous euchromatin and appeared mitochondria (M) and normal sized endoplasmic reticulum (ER). Scal bar= 5 μ m. (B) Dich/Sr group showing hepatic tissues Laceration with disappearance of most of hepatic structures and functional organelles (Red star), Appearance of nucleus in very necrotic form as a crescent form with unregularly boundaries (NN). Scale bar=5 μ m. (C) Dich/Ba group showing Degeneration of most hepatic structures with mild necrotic nucleus (IN) with appeared irregular boundaries (Orange arrow), appearance of degenerated endoplasmic reticulum (DER) and degenerated mitochondria (Red star) and appearance of red blood cells (Green arrow) and destingration of most hepatic tissues (**). Scale bar = 5 μ m. (D) Dich/Fe group showing disappearance of the nucleus which revealed the occurrence of apoptosis with appeared large sized red blood cells (Green arrow) with degeneration of most hepatic structures (**) with disappearance of mitochondria crista (Red star).Scale bar = 5 μ m.

(b) Transmission Electron microscopy of sections of (A) control heart showing Cardiomyocytes that have a tightly organized sarcomeric structure containing a peripheral nucleus with regular chromatin, the Z-lines are clearly visible (white arrow) and normal mitochondria are clearly cristal within myofiber (MI), and integrity intercalated disc (red arrow). Scale bar = 2 μ m. (B) Electron microscopy of sections from treated group with Dich/Sr showing the cardiomyocytes have a disorganized sarcomeric structure along with the appearance of intercellular spaces. In addition, another interesting observation was the abnormal accumulation of mitochondria within myofibers (**) and destroyed intercalated disc (Yellow arrow). Scale bar= 5 μ m. (C) Electron microscopy of section from treated group with Dich/Ba containing abnormal nucleus with irregular membrane and abnormal chromatin. Some fibers exhibited a complete lack of organization with Z-lines that appeared to be dissolving or fragmented and myofibrils and appeared lesion in cardiac myofibril (L) separated in fascicles by the sarcomeres (Red arrow). Scale bar= 5 μ m. (D) Electron microscopy of section from treated group with Dich/Fe showing Z-lines exhibited various types of morphologies, Some Z-lines were extremely thick (White arrow), rounded, and highly electron dense whereas others were punctate and appeared fragmented. Scale bar= 2 μ m.

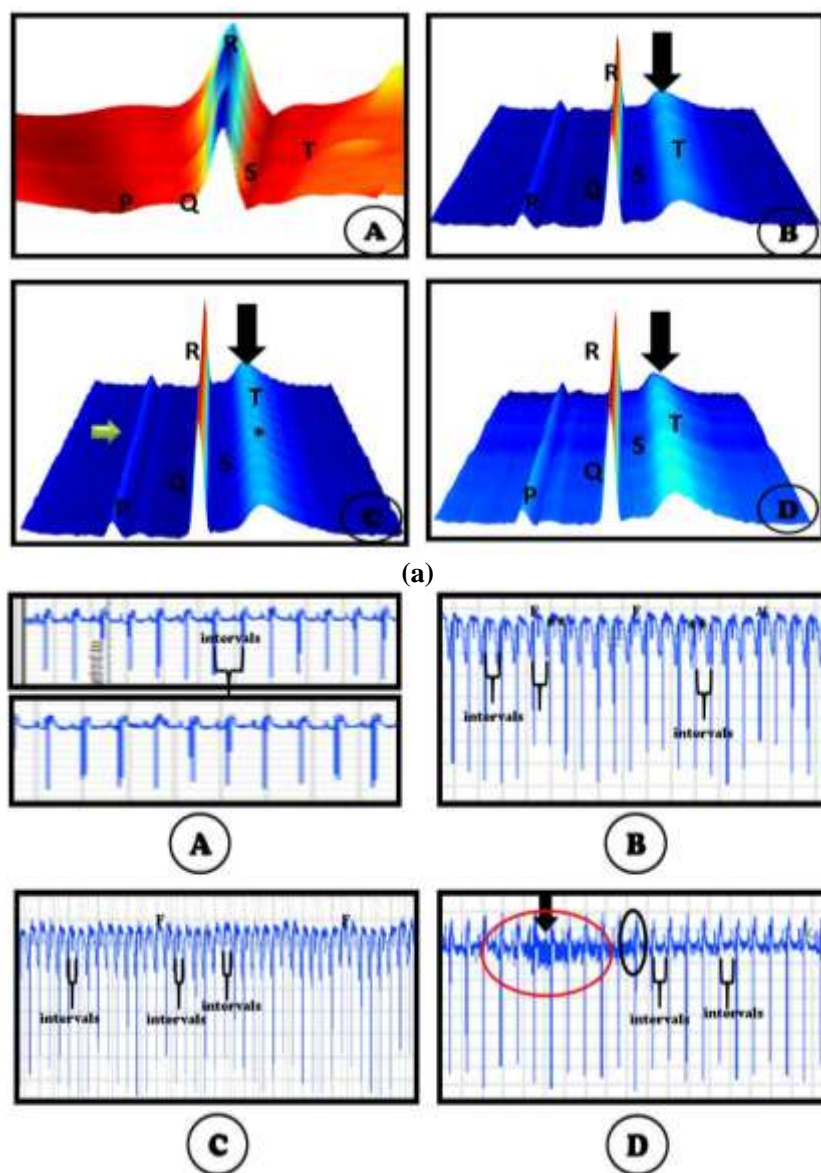


Fig. 7: (a) Illustrative 3D parametric ECG displays of radial velocity with the Lab chart software: control (A) Control group which showing normal heart beats with the characteristic points (P, Q, R, S, T) showing normal signal as (P) represent contraction of the heart and movement of blood from up down the heart, (QRS) represent the ventricle contraction and appear upper than other signals, (T) represent the relaxation of the heart and pulse end with normal waves and appearance of rich oxygenated red colour without waves with regular waves. (B) Dich/Sr group showing blue colour which indicates incidence of oxidative stress and wavy in (P and T) waves with appearance of faint blue colour which indicates cardiac cells necrosis and area of non-clearance flow. (C) Dich/Ba showing more wavy appearance of signals of heart with irregular waves in (P and T waves) (Green and Black arrows) that indicates up normal blood flow with faint colour in T wave which indicates necrotic cardiac tissues(*). (D) Dich/Fe showing irregular heartbeats waves (wavy chart) with high faint blue colour of T wave which indicates more cardiac damages.
(b) Electrocardiograms (ECG) changes in rats in different treated groups showing (A) in control group showing normal P waves with normal interval of 0.14 sec. (B) Dich/Sr treated group showing case of ventricular tachycardia as this chart is distinguished in diagnostic of ventricular tachycardia which showing ventricular aberration which occurs in short repeated bursts, separated by appeared two sinus (intervals black arrow) with appeared atrial flutter (F) which is recognized by the presence of "saw tooth" with average intervals of 0.10 sec. (C) Dich/Ba treated group showing treated group showing also a case of ventricular tachycardia with appeared ventricular aberration which occurs in this group by very short repeated bursts (very narrow peak), separated by appeared narrow two sinus (intervals black arrow) with appeared atrial flutter (F) which is recognized by the presence of "saw tooth" with average intervals of 0.8 sec. (D) Dich/Fe treated group showing high case of ventricular tachycardia which is known as (repetitive tachycardia) (Red circle) with short beat intervals (intervals black arrow) and appeared ventricular fusion beats (Black circle) as appeared the fusion of beats with average intervals of 0.9 sec.

Effect on expressions of inducible nitric oxide synthase (iNOS) and cyclooxygenase-2 (COX-2) at mRNA expression levels: NO is produced from L-arginine conversion to L-citrulline by iNOS⁴³ and mediated by COX-2⁴⁴. We hope to investigate whether the induction observed in the hepatic toxicity by novel complexes (Dich/Sr, Dich/Ba and Dich/Fe)-induced NO and PGE2 production (Fig. 8) was related to the modulation of iNOS and COX-2 using RT-PCR. The mRNA expression levels of iNOS and COX-2 were detected and undetectable in control group, whereas their levels markedly increased after treatment with these novel complexes (Dich/sr, Dich/Ba and Dich/Fe) (Fig. 8).

Effect on expressions of IL-1 β , TNF- α and IL-6 at mRNA expression levels: Interaction between the novel complexes (Dich/sr, Dich/Ba and Dich/Fe) and CD14 receptors caused the induction of pro-inflammatory cytokines including IL-1 β , TNF- α and IL-6⁴⁵. These cytokines have been considered as to investigate the inflammatory action of the novel complexes (Dich/sr, Dich/Ba and Dich/Fe), the inflammatory cytokines production was evaluated by RT-PCR. The IL-1 β , TNF- α and IL-6 mRNA levels were up-regulated in hepatic tissues in groups treated with the novel complexes (Dich/sr, Dich/Ba and Dich/Fe) compared with control untreated group (Fig. 6). The complexes (Dich/sr, Dich/Ba and Dich/Fe) caused a marked increment in IL-6, IL-1 β and TNF- α mRNA levels (Fig. 8), They also induced IL-1 β production.

Comet results: The comet assay data expressed as the tail moment and tail DNA % for heart were exposed to different doses of Dich/sr, Dich/Ba and Dich/Fe treated groups. Cells exposed to these novel complexes exhibited a significant increase in single-strand breaks. Comet images of cells derived from the heart showed the higher degree of damage with the appearance of more than one apoptotic cells with the large tail and small head and the relaxed loops of damaged DNA extend to form a comet-shaped structure (e-component).

Discussion

The current study is considered as a new strategy for incidence of severe hepatic damages by new complexity between 2,6 dichlorobenzene indophenol with Sr, Ba and Fe metals which will be turning points in the severe hepatotoxicity by new synthesized complexes and open new gate for the excellence in the experiments in this field of toxicology. In the gross section of hepatic tissues, the enlargement size of hepatic tissues appeared which is consistent with results of Daniel et al⁴⁶ who reported that the total body weight was affected by Dich novel complexes (Dich/Sr, Dich/Ba and Dich/Fe) treatment.

Histopathological examination of stained liver sections of Dich-treated animals showed centrilobular hepatocellular hypertrophy, karyomegaly and anisocytosis. These results were similar to those seen with other chlorobenzene isomers (penta- and hexa-) that have been studied⁴⁶. All the previous

finding were reported in the current study in addition to severe damages by appearance of nodules and dark black spots with rupture of most of hepatic structures as appearing in TEM and histological sections.

Dich had no effect on promoting GST level⁴⁶. This is in contrast to the current finding which confirmed the high effect of Dich/novel complexes (Dich/Sr, Dich/Ba and Dich/Fe) and induced significant decrement in all antioxidant enzymes (SOD, CAT and GRx) with marked elevation of marker of lipid peroxidation (MDA) which confirmed the high hepatotoxicity induced by the synthesized complexes. Under normal physiological conditions, transferrin-bound iron (TBI) is taken up by hepatocytes through an endocytic pathway involving the serum transferrin/transferrin receptor cycle.

Once in the cytosol, iron is rapidly directed to its functional sites, mainly in cell organelles, where it catalyses essential reactions. Excess iron is stored within a ferritin core. In addition to storage, endocytic and functional iron (~95% of cell iron), cytosolic iron and organelle catalytically-active iron loosely-bound to low molecular weight compounds (so called labile cellular iron, LCI), are "strategically" placed in key positions for iron metabolism⁴⁷. This explanation may give a logic explanation to the severe toxicity recorded in Dich/Fe treated group which showed severe damages represented by high liver enzymes (AST, ALT and LDH) and markers of tumor necrosis (TNF- α and AFP) and ultrastructural variation in hepatic tissues in addition to the presence of fragmented and myofibrils and expression of inflammatory markers.

The range-finding test and 90-day experiment of strontium chloride showed incidence of toxicity, only a few alterations were observed with little histopathological alterations as recorded by Kroes et al¹³ which is completely different from our current finding which proved the severe toxicity induced by novel complex of Dich/Sr showing damage effect on liver and ECG with appearance of atrial flutter and ventricular tachycardia, Declining antioxidant enzymes and elevating lipid peroxidation levels with high mitochondrial swelling and DNA damages appear clearly in expression of TNF- α , IL-6, IL-1 β , COX-2 and iNOS with degeneration of hepatic structures and rupture of cardiac bundles.

Dich/Ba novel complex induced severe hepatic and cardiotoxicity also as reported previously about barium chloride by Borzelleca et al⁹ who suggested that orally administered BaCl₂ may be nephrotoxic in rats based on their findings of related alterations in BUN. Additionally, renal failure in humans following a suicide attempt by BaCl₂ ingestion is also suggestive that the liver may be a target organ for Ba toxicity and this confirmed our study.

Although exposures to various chemicals including the heavy metals has been reported to trigger different sorts of toxicity⁴⁸, our studies represent further evidence that Ba

complexes with Dich induced sever damages and hepatotoxicity represented by high Troponin, CK, CK-MP levels, TNF- α , AFP, CRP and appearance of two sinus with

"saw tooth" and appearance of DNA as a comet like structure which confirmed the high toxicity induced by the novel complexes.

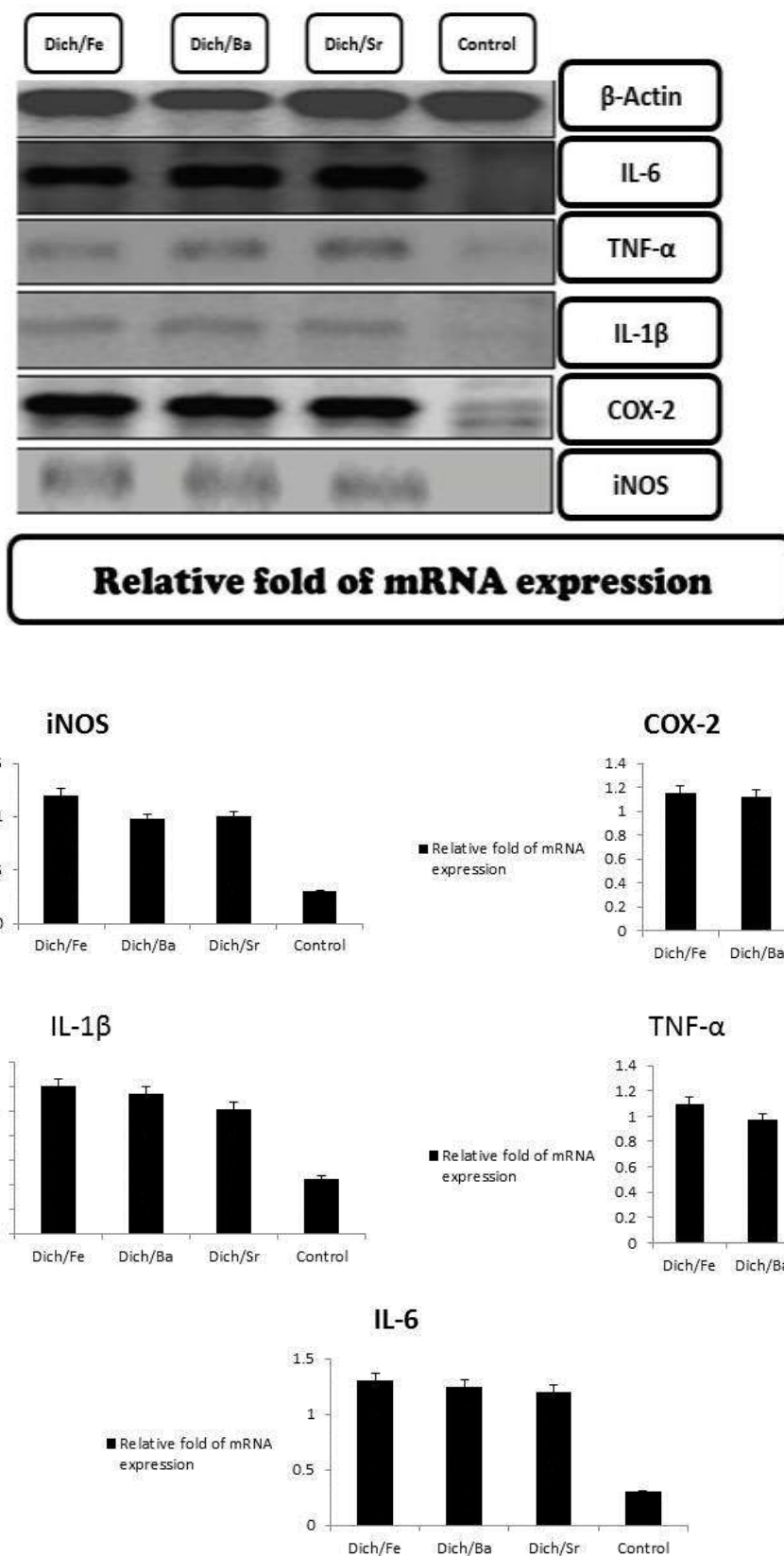


Fig. 8: Relative fold of mRNA expression of β -Actin, IL₆, TNF- α , IL-1 β , COX-2 and iNOS in treated groups

Conclusion

The current results proved that the synthesized novel complexes (Dich/Sr, Dich/Ba and Dich/Fe) succeeded greatly in inducing sever hepatic and cardiac toxicity with a lot of confirmation of analysis: physiological, biochemical, molecular, genetic, structural and ultrastructural results which confirmed the current novel concept and approved this new approach.

Acknowledgement

This work was supported by grants from Deanship of Scientific Research, Taif University, Saudi Arabia under Research Group Project Grants No. 6144-440-1.

References

1. Peattie M.E., Lindsay D.G. and Hoodless R.A., Dietary exposure of man to chlorinated benzenes in the United Kingdom, *Sci. Total Environ.*, **34**, 73–86 (1984)
2. Araya S.P., Mahajan M. and Jain P., Photometric Methods for the Determination of Vitamin C, *Anal Sci.*, **14**, 889–895 (1998)
3. US Department of Commerce, US exports, schedule E commodity by country (FT410: December 1980), Bureau of Census, Washington DC, 2–74 (1981)
4. Kulkarni S.G., Outcome of toxicity: toxicodynamic interaction of liver injury and repair, NLU Dissertation, 78–79 (1997)
5. Michalopoulos G.K., Liver regeneration: molecular mechanisms of growth control, *FASEB J.*, **4**, 176–187 (1990)
6. Valentovic M.A., Ball J.G., Anestis D. and Madan E., Acute hepatic and renal toxicity of dichlorobenzene isomers in Fischer 344 rats, *J. Appl. Toxicol.*, **13**, 1–7 (1993)
7. Brodie B.B., Reid W.D., Cho A.K., Sipes I.G., Krishna G. and Gillette J.R., Possible mechanisms of liver necrosis caused by aromatic organic compounds, *Proc. Natl. Acad. Sci., USA*, **68**, 160–164 (1971)
8. Pietrangelo A., Mechanisms of iron hepatotoxicity, *Journal of Hepatology*, **65**, 226–227 (2016)
9. Borzelleca J.F., Condie L.W. Jr. and Egle J.L. Jr., Short-term toxicity (one- and ten-day gavage) of barium chloride in male and female rats, *Journal of the American College of Toxicology*, **7**, 675–685 (1988)
10. Stokinger H.E., The metals, In Putty's Industrial Hygiene and TO-Xicology, Clayton G.D. and Clayton F.E., eds., Wiley, New York, 1531-1537 (1981)
11. Brenniman G.R., Kojola W.H., Levy P.S., Camow B.W. and Namekata T., High barium levels in public drinking water and its association with elevated blood pressure, *Arch Environ. Health*, **36**, 28-32 (1981)
12. Phelan D.M. and Hagley S.R., Is hypokalemia the cause of paralysis in barium poisoning?, *Br. Med. J.*, **289**, 882 (1984)
13. Kroes R., Den Tonkelaar S.M., Minerhoud A., Speijers G.J.A., Vonk-visser D.M.A., Berkvens J.M. and Van Esch G.J., Short toxicity of strontium chloride in rats, *Toxicology*, **7**, 11-21 (1977)
14. Gunawardhana L., Mobley S.A. and Sipes I.G., Modulation of 1,2- Dichlorobenzene hepatotoxicity in the Fischer- 344 rat by scavenger of superoxide Anions and an inhibitor of kupffer cells, *Toxicology and Applied Pharmacology*, **119**, 205-213 (1993)
15. Bradford M.M., A rapid and sensitive method for the quantitation of microgram quantities of protein utilizing the principle of protein-dye binding, *Anal. Biochem*, **72**, 248-54 (1976)
16. King J., The transferases alanine and aspartate transaminases, In Practical clinical enzymology, London, Van Nostrand Company Limited, 121-138 (1965)
17. Kaplan A. and Szalbo J., Clinical chemistry: Interpretation and techniques, 2nd ed., Kaplan A. and Szabo J., editors, 157 (1983)
18. Wener M.H., Daum P.R. and McQuillin G.M., The influence of age, sex and race on the upper reference limit of serum C-reactive protein concentration, *J. Rheumatol.*, **27(10)**, 2351-2359 (2000)
19. Aebi H., Catalase *in vitro*, *Meth. Enzymol*, **105**, 121 –126 (1984)
20. Marklund S. and Marklund G., Involvement of the superoxide anion radical in the autoxidation of pyrogallol and a convenient assay for superoxide dismutase, *J Biochem*, **47**, 469-74 (1974)
21. Ohkawa H., Ohishi N. and Yagi K., Assay for lipid peroxides in animal tissues by thiobarbituric acid reaction, *Anal. Biochem.*, **95**, 351 (1979)
22. Couri D. and Abdel-Rahman M.S., Effect of chlorine dioxide and metabolites on glutathione dependent system in rat, mouse and chicken blood, *J. Environ. Pathol. Toxicol.*, **3**, 451-460 (1979)
23. Goldberg D.M. and Spooner R.J., Methods of enzymatic analysis, Bergmeyer H.V., ed., 3rd ed., **3**, 258-265 (1983)
24. Suzuki K., Ota H., Sasagawa S., Sakatani T. and Fujikura T., Assay method for myeloperoxidase in human polymorphonuclear leukocytes, *Anal Biochem*, **132**, 345–352 (1983)
25. Litwack G., Bothwell J.W., Williams J.N. and Elvehjem C.A., A colorimetric assay for xanthine oxidase in rat liver homogenates, *J Biol Chem*, **200**, 303–310 (1953)
26. Zhao Y. et al, Vanadium compounds induced mitochondria permeability transition pore (PTP) opening related to oxidative stress, *J Inorg Biochem.*, **104**, 371-8 (2010)
27. Ayoubi M. et al, Biochemical mechanisms of dose-dependent cytotoxicity and ROS-mediated apoptosis induced by lead sulfide/graphene oxide quantum dots for potential bioimaging applications, *Sci Rep.*, **7**, 12896 (2017)
28. Naserzadeh P. et al, Single-walled carbon nanotube, multiwalled carbon nanotube, and Fe₂O₃ nanoparticles induced mitochondria-mediated apoptosis in melanoma cells, *Cutan Ocul Toxicol.*, **37**, 157-66 (2018)

29. Tafreshi N., Hosseinkhani S., Sadeghizadeh M., Sadeghi M., Ranjbar B. and Naderi-Manesh H., The influence of insertion of a critical residue (Arg356) in structure and bioluminescence spectra of firefly luciferase, *J Biol Chem.*, **282**, 8641-7 (2007)
30. Salimi A., Vaghar-Moussavi M., Seydi E. and Pourahmad J., Toxicity of methyl tertiarybutyl ether on human blood lymphocytes, *Environ Sci Pollut Res Int.*, **23**, 8556-64 (2016)
31. Zhang F., Xu Z., Gao J., Xu B. and Deng Y., In vitro effect of manganese chloride exposure on energy metabolism and oxidative damage of mitochondria isolated from rat brain, *Environ Toxicol Pharmacol.*, **26**, 232-6 (2008)
32. Gabe M., Techniques histologiques, Histological Techniques, Paris, Masson Publisher (1968)
33. Weakley B. and Beginner S., Handbook of Biological Transmission Electron Microscopy, 2nd Churchill Livingstone, London (1981)
34. Endoh D., Okui T., Ozawa S., Yamato O., Kon Y. and Arikawa Hayashi M., Protective effect of a lignan-containing flaxseed extract against CCl₄-induced hepatic injury, *Journal of Veterinary Medical Science*, **64**, 761-765 (2002)
35. Geary W.J., The Use of Conductivity Measurements in Organic Solvents for the Characterisation of Coordination Compounds, *Coord. Chem. Rev.*, **7**, 81 (1971)
36. Nakamoto K., Infrared and Raman Spectra of Inorganic and Coordination Compounds, Wiley, New York (1986)
37. Thomas M., Nair M.K.M. and Radhakrishnan P.K., Rare Earth Iodide Complexes of 4-(2',4'-Dihydroxyphenylazo) Antipyrine, *Synth. React. Inorg. Met. Org. Chem.*, **25**, 471 (1995)
38. Bellamy L.J., The Infrared Spectra of Complex Molecules, Second ed., Chapman & Hall, Methuen, London (1958)
39. Yohannan Panicker C., Tresa Varghese H. and Philip D., FT-IR, FT-Raman and SERS spectra of vitamin C. *Spectrochimica Acta Part A, Molecular and Biomolecular Spectroscopy*, **65**(3-4), 802-804 (2006)
40. Coates J., Interpretation of infrared spectra, a practical approach, In *Encyclopedia of Analytical Chemistry*, Meyers R.A., ed., John Wiley & Sons Ltd., Chichester, 10815-10837 (2000)
41. Lever A.B.P., Electronic spectra of dn ions *Inorganic electronic spectroscopy*, 2nd ed. (1984)
42. Cotton F.A. and Wilkinson G., The element of first transition series, *Advanced inorganic chemistry*, 3rd ed. (1992)
43. Allerton T.D., Proctor D.N., Stephens J.M., Dugas T.R., Spielmann G. and Irving B.A., l-Citrulline Supplementation: Impact on Cardiometabolic Health, *Nutrients*, **10**, <https://doi.org/10.3390/nu10070921> (2018)
44. Chizzolini C. and Brembilla N.C., Prostaglandin E2: igniting the fire, *Immunol Cell Biol.*, **87**, 510-511, <https://doi.org/10.1038/icb.2009.56> (2009)
45. Mackman M., How do oxidized phospholipids inhibit LPS signaling?, *Arterioscler. Thromb. Vasc Biol.*, **23**, 1133-1136 (2003)
46. Daniel L. et al, Use of a medium-term liver focus bioassay to assess the hepatocarcinogenicity of 1,2,4,5-tetrachlorobenzene and 1,4-dichlorobenzene, *Cancer Letters*, **129**, 39-44 (1998)
47. Fader Kelly A., Nault Rance, Kirby Mathew P., Markous Gena, Matthews Jason and Zacharewski Timothy R., Convergence of hepcidin deficiency, systemic iron overloading, heme accumulation and REV-ERB α/β activation in aryl hydrocarbon receptor-elicited hepatotoxicity, *Toxicology and Applied Pharmacology*, **321**, 1-17 (2017)
48. Hook J.B. and Hewitt W.R., Toxic responses of the kidney. In Casarett and Doall's *Toxicology the Basic Science of Poisons*, Klaassen C.D., Amdur M.O. and Doull J., eds., 3rd ed., Macmillan Co., New York, Chap. 11, 310-329 (1986).

(Received 31st October 2020, accepted 05th December 2020)